Proceedings of the ASME 2012 International Symposium on Flexible Automation
ISFA 2012
June 18-20, 2012, St. Louis, Missouri, USA

ISFA2012-7199

A TWO-STAGE MODEL BASED ITERATIVE LEARNING CONTROL SCHEME FOR A CLASS OF MIMO MISMATCHED LINEAR SYSTEMS *

Wenjie Chen
Department of Mechanical Engineering
University of California
Berkeley, California 94720
Email: wjchen@me.berkeley.edu

Masayoshi Tomizuka
Department of Mechanical Engineering
University of California
Berkeley, California 94720
Email: tomizuka@me.berkeley.edu

ABSTRACT

This paper discusses the tracking control problem for a class of multi-input-multi-output (MIMO) mismatched linear systems, where there are disturbances in different channels from the control input and the real-time feedback signal is not the output of interest. This mismatch makes it difficult to achieve high tracking performance for the interested output. To address this problem, two model based iterative learning control (ILC) algorithms, namely reference ILC and torque ILC, are designed for different injection locations in the closed loop system. An ad hoc hybrid scheme is proposed to make transitions between the two ILC stages for them to work properly at the same time. The proposed scheme is validated through the experimental study on a single-joint indirect drive system.

INTRODUCTION

In industrial applications, the automated system (e.g., the robotic manipulator) is often required to repeatedly perform a single task under the same operating conditions. If the system repeatability is good, the trajectory tracking error will become repetitive from one run to another. In this case, the iterative learning control (ILC) scheme is well suited to compensate for the repeatable tracking error [1, 2].

Iterative learning control is a data-driven methodology which iteratively utilizes the data (e.g., error profile) from previous trails to update the system inputs for the next iteration. Many variations of the ILC scheme have been studied for various applications [1]. Most of them, however, are developed for the fundamental case where the system has direct measurement of the interested output for real-time feedback and does not have disturbances in the channels different from the control input. Therefore, in mismatched systems where the above scenario does not hold, the standard ILC performance will be limited and in some cases the ILC convergence is hard to guarantee.

The mismatched systems discussed in this paper are common in practical applications, e.g., the industrial robots with indirect-drive joint mechanisms (joints with elasticity). Several feedback control approaches, such as integrator backstepping [3], dynamic surface control [4], and adaptive robust control [5], have been developed specifically to deal with these mismatched systems. Some efforts have been devoted to migrating these ideas to the field of ILC to deal with the mismatched uncertainty iteratively while exploiting the noncausal repetitiveness. A two-stage ILC approach was proposed in [6] to deal with robots with joint elasticity. Similar to backstepping, the real-time measured output (i.e., motor side state) is utilized in [6] as a hypothetical input to control the output of interest (i.e., load side state). As shown later in this paper, the convergence rate of this learning process may be adversely affected and thus the use of a high bandwidth Q filter to learn high frequency error may compromise stability. Other studies such as [7] also reported the compromise on the tracking performance they had to make for a better learning convergence. This is especially the case when the system exhibits mismatched uncertainties. Regarding this stabil-

*THIS WORK WAS SUPPORTED BY FANUC LTD., JAPAN. REAL-TIME CONTROL HARDWARE AND SOFTWARE WERE PROVIDED BY NATIONAL INSTRUMENTS, INC.

ity issue under uncertainty, various robust approaches have been proposed [8, 9]. The resulting algorithms are usually nontrivial and the performance is normally compromised for a conservative robust controller. In [9], it requires the plant resonances to be suppressed by feedback compensation in order for the proposed method to improve the robustness to high-frequency modeling errors. In [10], a model-based ILC approach was developed for elastic robots to learn the error component beyond the first resonant frequency. However, this approach requires an accurate piecewise-linear model to be identified and interpolated for each trajectory in advance, which limits its application.

This paper will propose a hybrid two-stage model-based ILC approach for a class of MIMO mismatched linear systems. The two-stage ILC is aimed to push the learning algorithm to a higher bandwidth while maintaining the fast model-based convergence rate. The paper is organized as follows. The system model and the basic controller structure are introduced first. Then two ILC schemes are designed independently followed by an ad hoc hybrid scheme to enable the two ILC schemes to execute simultaneously. The experimental study on a single-joint indirect drive system is presented next to validate the effectiveness of the proposed scheme. The parametric uncertainty and mismatched dynamics such as various disturbances at different locations of the system will be addressed. The conclusions of this work will be given at last.

SYSTEM OVERVIEW

System Model

Consider a MIMO mismatched linear system in the following discrete time state space form

$$x(j+1) = Ax(j) + B_u u(j) + B_d d(j) \tag{1}$$

$$y(j) = \left[q_m^{\mathrm{T}}(j),\, q_\ell^{\mathrm{T}}(j)\right]^{\mathrm{T}} = Cx(j) + D_u u(j) + D_d d(j) \tag{2}$$

where j is the time step index. $x \in \mathbb{R}^{n_x}$ is the system state, $u \in \mathbb{R}^{n_u}$ is the control input, $d \in \mathbb{R}^{n_d}$ is the lumped disturbance, $q_m \in \mathbb{R}^{n_m}$ and $q_\ell \in \mathbb{R}^{n_\ell}$ are the two outputs of the plant. d is regarded as the mismatched uncertainty/disturbance if it (or part of it) is applied to different channels from the control input u (i.e., $B_u \neq \alpha B_d, \forall \alpha \in \mathbb{R}$). Another mismatched assumption is that, only part of the outputs (i.e., q_m) is measured for real-time feedback, even if the output of interest may be q_ℓ. However, the measurement of q_ℓ may be available for iteration based off-line use. Furthermore, besides the unknown mismatched dynamics, it is assumed that parametric uncertainties exist in the available nominal model.

This system can be reformulated as

$$q_m(j) = P_{mu}(z)u(j) + P_{md}(z)d(j) \tag{3}$$

$$q_\ell(j) = P_{\ell u}(z)u(j) + P_{\ell d}(z)d(j) \tag{4}$$

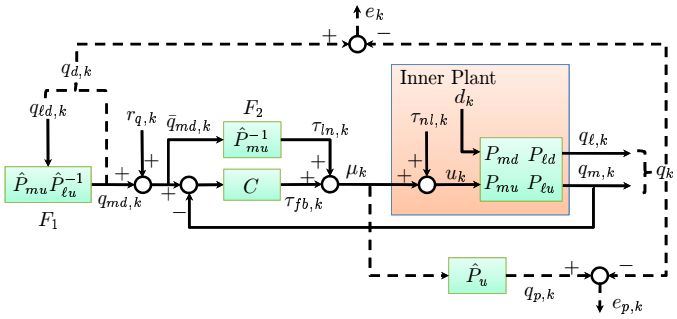

FIGURE 1. Control Structure with Reference & Torque Update

where P_{mu}, P_{md}, $P_{\ell u}$, and $P_{\ell d}$ are the transfer functions from u or d to the corresponding output. For simplicity, the following control scheme is formulated for the case where P_{mu} and $P_{\ell u}$ are diagonal matrices. However, it may be possible to extend this work to a more general case by considering the plant inversion and commutative multiplication for the non-diagonal matrices.

Basic Controller Structure

Figure 1 illustrates the control structure for this mismatched system, where the subscript k is the iteration index. It consists of two feedforward controllers, F_1 and F_2, and one feedback controller, C. Here, C can be any linear feedback controller such as a decoupled PID controller to stabilize the system. The feedforward controllers, F_1 and F_2, are designed using the nominal inverse model as

$$q_{md,k}(j) = \hat{P}_{mu}(z)\hat{P}_{\ell u}^{-1}(z)q_{\ell d,k}(j) \triangleq F_1(z)q_{\ell d,k}(j) \tag{5}$$

$$\tau_{ln,k}(j) = \hat{P}_{mu}^{-1}(z)\left[q_{md,k}(j) + r_{q,k}(j)\right] \triangleq F_2(z)\bar{q}_{md,k}(j) \tag{6}$$

where $\hat{\bullet}$ is the nominal model representation of $\bullet$. $q_{\ell d,k}$ is the desired plant output for $q_{\ell,k}$. $r_{q,k}$ and $\tau_{nl,k}$ are used as the additional reference and feedforward torque updates generated iteratively by the two-stage ILC algorithm designed later.

TWO-STAGE ILC SCHEME

ILC Basics

Some basics of the general ILC scheme are reviewed first, which will be utilized in the subsequent ILC scheme design. Consider the MIMO linear system with the error dynamics and the ILC law in the following form

$$\bar{e}_k(j) = -P_{eu}(z)\bar{u}_k(j) + \bar{r}(j) \tag{7}$$

$$\bar{u}_{k+1}(j) = Q(z)\left[\bar{u}_k(j) + L(z)\bar{e}_k(j)\right] \tag{8}$$

where $\bar{e}$ is the error that the ILC scheme aims to reduce, $\bar{r}$ is the lumped repetitive reference and/or disturbance input to the

system, and $\bar{u}$ is the control input updated iteratively by the ILC scheme using the filters $L(z)$ and $Q(z)$. Similar to [1, 11], the following convergence property holds:

Theorem 1. *The ILC system* (7)-(8) *is monotonically and exponentially convergent in the sense that* $\|\bar{u}_k - \bar{u}_\infty\|_p \to 0$ *and* $\|\bar{e}_k - \bar{e}_\infty\|_p \to 0$ *as* $k \to \infty$, *if*

$$\beta = \|Q(z)\left[I - L(z)P_{eu}(z)\right]\|_p < 1 \tag{9}$$

where β *is the rate of convergence,* I *is the identity matrix with appropriate dimension, the p-norm* $\|\bullet\|_p = (\sum_i |\bullet_i|^p)^{1/p}$, *and*

$$\bar{u}_\infty(j) = \left[I - Q(z) + Q(z)L(z)P_{eu}(z)\right]^{-1} Q(z)L(z)\bar{r}(j) \tag{10}$$
$$\bar{e}_\infty(j) = \left[I - Q(z) + Q(z)L(z)P_{eu}(z)\right]^{-1} \left[I - Q(z)\right]\bar{r}(j) \tag{11}$$

Proof. First, with (7) and (8), it is easy to see that

$$\bar{u}_{k+1}(j) = Q(z)\left[I - L(z)P_{eu}(z)\right]\bar{u}_k(j) + Q(z)L(z)\bar{r}(j) \tag{12}$$

which yields

$$\begin{aligned}\|\bar{u}_{k+1} - \bar{u}_\infty\|_p &= \|Q(z)\left[I - L(z)P_{eu}(z)\right](\bar{u}_k - \bar{u}_\infty)\|_p \\ &\le \|Q(z)\left[I - L(z)P_{eu}(z)\right]\|_p \|\bar{u}_k - \bar{u}_\infty\|_p \end{aligned} \tag{13}$$

Therefore, if $\|Q(z)\left[I - L(z)P_{eu}(z)\right]\|_p < 1$, $\|\bar{u}_k - \bar{u}_\infty\|_p \to 0$ as $k \to \infty$. With (7), similar conclusion can be drawn for the convergence of $\bar{e}_k$. Note that the inverse $\left[I - Q(z) + Q(z)L(z)P_{eu}(z)\right]^{-1}$ exists because $\|Q(z)[I - L(z)P_{eu}(z)]\|_p < 1$. □

Equation (11) shows that the steady state error $\bar{e}_\infty$ vanishes with complete learning (i.e., $Q(z) = I$), which means the effects on $\bar{e}_\infty$ from the repetitive input $\bar{r}$ will be fully compensated. The ILC law (8) implies the Q filter can also be used to shape the learning ability in the frequency domain. In order to achieve better performance, it is desired to push the bandwidth of $Q(z)$ to be as high as possible. Equation (9), however, indicates that the bandwidth of $Q(z)$ may have to be compromised to ensure monotonic convergence and to avoid poor transients in the learning process. In practice, a low-pass filter $Q(z)$ is typically employed to prevent the effects of high frequency model uncertainties from entering the learning process [1]. Also, $Q(z)$ should be unity gain at low frequencies where complete learning is preferred to achieve zero steady state error. Since the ILC scheme is an offline iteration based method, acausal filtering can be utilized to obtain a zero-phase learning response.

Given a fixed Q filter, the optimal learning filter to achieve the fastest convergence is obtained as

$$L^*(z) = \arg\min_{L(z)} \|Q(z)\left[I - L(z)P_{eu}(z)\right]\|_p \tag{14}$$

This leads to the plant inversion choice, i.e., $L^*(z) = P_{eu}^{-1}(z)$. This model matching problem can be solved with many optimization techniques, such as the H_∞ synthesis [8], if the model uncertainty bound is known. The designed $Q(z)$ and $L(z)$ need to be validated using (9) with the knowledge of system model uncertainty. Without loss of generality, the optimal learning filter in this paper is simply chosen as $L^*(z) = \hat{P}_{eu}^{-1}(z)$.

ILC With Reference Update

Denote the sensitivity function of the closed loop system in Fig. 1 as $S_p(z) = \left[I + C(z)P_{mu}(z)\right]^{-1}$. From (5), $q_{md,k}$ is related to $q_{d,k}$ (i.e., $q_{\ell d,k}$ or $q_{md,k}$) as follows

$$q_{md,k} = \hat{P}_{mu}\hat{P}_u^{-1} q_{d,k} \tag{15}$$

where P_u can be either P_{mu} or $P_{\ell u}$ depending on the choice of $q_{d,k}$. The time index j for all signals and the discrete time operator z for all transfer functions are omitted hereafter for simplicity. The system output q_k (i.e., $q_{m,k}$ or $q_{\ell,k}$) can be derived as

$$\begin{aligned} q_k &= P_u u_k + P_d d_k \\ &= P_u S_p\left[(C + \hat{P}_{mu}^{-1})(q_{md,k} + r_{q,k}) + \tau_{nl,k} - CP_{md}d_k\right] + P_d d_k \\ &= \hat{P}_{mu}^{-1}P_u S_p \hat{S}_p^{-1} r_{q,k} + P_u S_p\left(\hat{P}_u^{-1}\hat{S}_p^{-1} q_{d,k} + \tau_{nl,k} - CP_{md}d_k\right) + P_d d_k \end{aligned} \tag{16}$$

The corresponding tracking error e_k is

$$\begin{aligned} e_k = q_{d,k} - q_k &= -\hat{P}_{mu}^{-1}P_u S_p \hat{S}_p^{-1} r_{q,k} + (I - P_u S_p \hat{P}_u^{-1}\hat{S}_p^{-1}) q_{d,k} \\ &\quad - P_u S_p \tau_{nl,k} + (P_u S_p C P_{md} - P_d) d_k \\ &\triangleq -P_{eu,r} r_{q,k} + \bar{r}_{r,k} \end{aligned} \tag{17}$$

The tracking performance of the next iteration can be improved with the reference update scheme (namely reference ILC (L) or reference ILC (M) depending on the choice of e_k) as

$$r_{q,k+1} = Q_r(r_{q,k} + L_r e_k) \tag{18}$$

Assume the desired trajectory $q_{d,k}$, the feedforward torque update $\tau_{nl,k}$, and the disturbance d_k are repetitive for each iteration. From Theorem 1, the monotonic convergence of this ILC scheme (18) can be guaranteed if $\beta_r = \left\|Q_r(1 - L_r\hat{P}_{mu}^{-1}P_u S_p \hat{S}_p^{-1})\right\|_\infty < 1$. With the inversion of the nominal model in (17), the optimal learning filter and the convergence rate are obtained as

$$L_r^* = \hat{P}_{eu,r}^{-1} = \hat{P}_u^{-1}\hat{P}_{mu} \tag{19}$$
$$\beta_r^* = \left\|Q_r(I - \hat{P}_u^{-1}P_u S_p \hat{S}_p^{-1})\right\|_\infty < 1 \tag{20}$$

and with complete learning (i.e., $Q_r = I$), the tracking error e_∞ vanishes. In order to achieve fast convergence rate without compromising the bandwidth of Q_r, it is desired to reduce the model uncertainties. This can be done by either obtaining a nominal model $\hat{P}_u$ more accurately representing the actual physical plant, or in contrast, making the inner plant (blue shaded area in Fig. 1) behave as the chosen nominal model $\hat{P}_u$. In the next section, an ILC scheme with torque update is introduced to achieve the latter objective, i.e., making $q_k \to \hat{P}_u \mu_k$, where $\mu_k = \tau_{ln,k} + \tau_{fb,k}$ is the torque input to the inner plant.

ILC With Torque Update

Define $e_{p,k}$ as the model following error between the nominal plant output (i.e., $q_{p,k} \triangleq \hat{P}_u \mu_k$) and the actual plant output q_k (i.e., $q_{\ell,k}$ or $q_{m,k}$). The ILC scheme to reduce this model following error $e_{p,k}$ can be formulated as

$$e_{p,k} = \hat{P}_u \mu_k - q_k \triangleq q_{p,k} - q_k \tag{21}$$

$$\tau_{nl,k+1} = Q_u \left(\tau_{nl,k} + L_u e_{p,k} \right) \tag{22}$$

where $\hat{P}_u$ is $\hat{P}_{\ell u}$ or $\hat{P}_{mu}$ to match with the choice of q_k. The corresponding ILC is termed as torque ILC (L) or torque ILC (M).

It shows that $\tau_{nl,k}$ is used to cancel out the effects on q_k from model uncertainty $\Delta P \triangleq P_u - \hat{P}_u$ and mismatched disturbance d_k. The ideal $\tau^*_{nl,k}$ to achieve this objective can be derived as

$$\begin{aligned} & \hat{P}_u \mu_k = P_u(\mu_k + \tau^*_{nl,k}) + P_d d_k \\ \Rightarrow \quad & \tau^*_{nl,k} = -P_u^{-1}(\Delta P \mu_k + P_d d_k) \end{aligned} \tag{23}$$

In the mismatched systems, the two objectives, following $\hat{P}_{mu}$ (i.e., torque ILC (M)) and following $\hat{P}_{\ell u}$ (i.e., torque ILC (L)), cannot be reached simultaneously (i.e., $\tau^*_{nl,mk} \neq \tau^*_{nl,\ell k}$), since $P_{mu}^{-1} P_{md} \neq P_{\ell u}^{-1} P_{\ell d}$ and $P_{mu}^{-1} \Delta P_m \neq P_{\ell u}^{-1} \Delta P_\ell$ in general. This means at this stage it is desired to select the nominal model to match with the chosen one in the reference ILC stage.

Convergence of Model Following Error The input-output equation of the nominal plant can be derived as

$$\begin{aligned} q_{p,k} &\triangleq \hat{P}_u \mu_k \\ &= \hat{P}_u S_p \left[(C + \hat{P}_{mu}^{-1})(q_{md,k} + r_{q,k}) - C P_{mu} \tau_{nl,k} - C P_{md} d_k \right] \end{aligned} \tag{24}$$

Then from (16) and (24), the model following error $e_{p,k}$ becomes

$$\begin{aligned} e_{p,k} = q_{p,k} - q_k &= -T_u S_p \tau_{nl,k} - \Delta P S_p (C + \hat{P}_{mu}^{-1})(q_{md,k} + r_{q,k}) \\ &\quad + (\Delta P S_p C P_{md} - P_d) d_k \\ &\triangleq -P_{eu,u} \tau_{nl,k} + \bar{r}_{u,k} \end{aligned} \tag{25}$$

where $T_u = \hat{P}_u C P_{mu} + P_u$.

Therefore, if the desired trajectory $q_{md,k}$, the reference update $r_{q,k}$, and the disturbance d_k remain the same for each iteration, by Theorem 1, the torque ILC scheme (22) will be monotonically converging if $\beta_u = \left\| Q_u (I - L_u T_u S_p) \right\|_\infty < 1$. By using the nominal plant inversion, the optimal choice of L_u with deadbeat convergence rate β_u^* becomes

$$L_u^* = \hat{P}_{eu,u}^{-1} = \hat{S}_p^{-1} \hat{T}_u^{-1} = \hat{P}_u^{-1} \tag{26}$$

$$\beta_u^* = \left\| Q_u \left(I - P_u \hat{P}_u^{-1} \right) S_p \right\|_\infty < 1 \tag{27}$$

and with complete learning (i.e., $Q_u = I$), the inner plant behaves like the nominal model as the model following error $e_{p,\infty} \to 0$.

Convergence of Tracking Error Using (17) and (25), the tracking error e_k can be derived as

$$\begin{aligned} e_k = P_u T_u^{-1} \cdot \Big[& e_{p,k} + \hat{P}_{mu} C \left(P_u^{-1} P_{mu} \hat{P}_u \hat{P}_{mu}^{-1} - I \right) q_{d,k} \\ & - \left(\hat{P}_{mu}^{-1} + C \right) \hat{P}_u r_{q,k} + C \hat{P}_u \left(P_{md} - P_d P_{mu} P_u^{-1} \right) d_k \Big] \end{aligned} \tag{28}$$

By assumption, $q_{d,k}$, $r_{q,k}$, and d_k do not vary from one iteration to another. Thus the tracking error e_k will also converge monotonically with the rate of $\beta_e \leq \| P_u T_u^{-1} \|_\infty \beta_u$ if the model following error $e_{p,k}$ converges and $P_u T_u^{-1}$ is BIBO stable.

Note that for torque ILC (M), $P_u^{-1} P_{mu} \hat{P}_u \hat{P}_{mu}^{-1} - I = 0$ and $P_{md} - P_d P_{mu} P_u^{-1} = 0$, which further reduces (28) to

$$e_k = P_u T_u^{-1} \left[e_{p,k} - (\hat{P}_{mu}^{-1} + C) \hat{P}_u r_{q,k} \right] \tag{29}$$

Thus if $r_{q,k} = 0$ (i.e., the reference ILC is not activated), $e_k \to 0$ as $e_{p,k}$ vanishes. For torque ILC (L), this is not true due to the mismatched behavior. The remaining tracking error e_∞ is

$$\begin{aligned} e_\infty = P_u T_u^{-1} \Big[& \hat{P}_{mu} C \left(P_u^{-1} P_{mu} \hat{P}_u \hat{P}_{mu}^{-1} - I \right) q_{d,\infty} \\ & - (\hat{P}_{mu}^{-1} + C) \hat{P}_u r_{q,\infty} + C \hat{P}_u (P_{md} - P_d P_{mu} P_u^{-1}) d_\infty \Big] \\ \triangleq & -P_{eu,ur} r_{q,\infty} + \bar{r}_{ur,\infty} \end{aligned} \tag{30}$$

which can be further eliminated through the reference ILC using $L_r^* = \hat{P}_{eu,ur}^{-1} = \hat{P}_u^{-1} \hat{P}_{mu}$, and this matches with (19).

Hybrid Scheme With Two-Stage ILC

In general, for the closed loop system with a satisfactory feedback controller, the sensitivity function S_p will behave as a high-pass filter to mitigate the low frequency error. Therefore,

in the convergence condition (27), the low frequency model uncertainty is greatly suppressed by S_p. This allows Q_u to have higher bandwidth without worrying about the low frequency uncertainty. Then with the effects of the torque ILC, the inner plant will behave like the nominal model (i.e., $q_k \to \hat{P}_u \mu_k$) up to the bandwidth of Q_u. Within this frequency range, the convergence condition of the reference ILC (20) will be simplified to

$$\beta_r \approx \left\| Q_r \left(I - S_p \hat{S}_p^{-1} \right) \right\|_\infty < 1 \tag{31}$$

which allows to push Q_r to a higher bandwidth for better tracking performance.

Note that the repetitive assumption is used in the derivation of the aforementioned two ILC schemes. When these two ILC schemes are activated simultaneously, the repetitive assumption will be no longer valid (i.e., $r_{q,k}$ and $\tau_{nl,k}$ are not repetitive from one iteration to another). Therefore, an ad hoc hybrid scheme is designed to reduce the adverse interference of the two ILC stages. Specifically, an iteration-varying gain is applied to each ILC stage as follows

$$\tau_{nl,k+1} = Q_u \left(\tau_{nl,k} + \gamma_{u,k} L_u e_{p,k} \right) \tag{32}$$

$$r_{q,k+1} = Q_r (r_{q,k} + \gamma_{r,k} L_r e_k) \tag{33}$$

where the two gains $\gamma_{u,k}$ and $\gamma_{r,k}$ can be tuned by trial and error, e.g., $\gamma_{u,k} = \min(4\frac{\sum_j \|e_{p,k}(j)\|_2}{\sum_j \|e_{p,1}(j)\|_2}, 1)$ and $\gamma_{r,k} = 1 - \frac{1}{2}\gamma_{u,k}$. The basic idea behind is that the torque ILC needs to take more effects whenever the model following error becomes larger in the previous iteration (i.e., $\frac{\sum_j \|e_{p,k}(j)\|_2}{\sum_j \|e_{p,1}(j)\|_2}$ increases). In order for the torque ILC to perform better, the effects of the reference ILC is accordingly attenuated with a decreased $\gamma_{r,k}$. In contrast, once the model following error is sufficiently small (i.e., the inner plant behaves as the nominal model), the torque ILC becomes not necessary and the reference ILC can be fully activated.

As shown in (29), for the application of tracking q_m, the reference ILC is not necessary and the torque ILC (M) with $\hat{P}_u = \hat{P}_{mu}$ will be sufficient. In order to track q_ℓ, however, the aforementioned hybrid two-stage ILC scheme with $\hat{P}_u = \hat{P}_{\ell u}$ will be necessary. And it is understood that the nominal models used in two ILC stages should match with each other due to the mismatched dynamics. In the experimental study, the algorithm validation will focus on the case of tracking q_ℓ to test the effectiveness of the hybrid two-stage ILC scheme.

EXPERIMENTAL STUDY

Experimental Setup & Dynamic Model

The proposed method is validated on a single-joint indirect drive robot shown in Fig. 2. This experimental setup consists of:

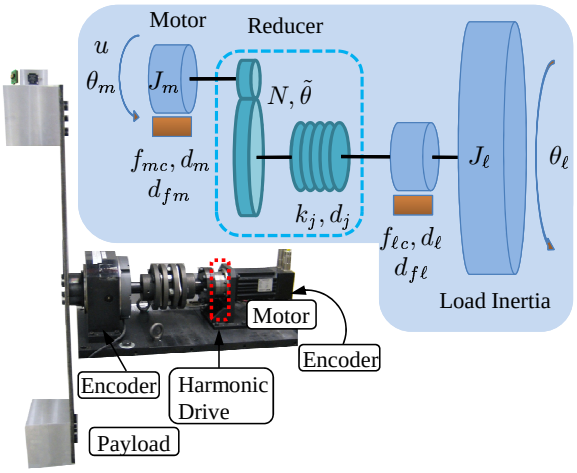

FIGURE 2. Single-Joint Indirect Drive System Setup

1) a servo motor with a 20,000 counts/revolution encoder, 2) a harmonic drive with a 80:1 gear ratio, 3) a load side 144,000 counts/revolution encoder, and 4) a payload. The anti-resonant and resonant frequencies of the setup are approximately 11Hz and 19Hz. It is assumed that the load side encoder measurement is only available for iteration based offline use rather than for real-time feedback use. Finally, the algorithms are implemented using a 1kHz sampling rate in a LabVIEW real-time target installed with LabVIEW Real-Time and FPGA modules.

Figure 2 also illustrates the schematic of the single-joint indirect drive mechanism. The subscripts m and ℓ denote the motor side and the load side quantities, respectively. θ represents the angular position and J is the moment of inertia. u is the motor torque input. d_m and d_ℓ represent the viscous damping coefficients at the motor side and the load side, respectively. k_j and d_j are the stiffness and the damping coefficients of the reducer. The gear ratio of the reducer is denoted by N. f_{mc} and $f_{\ell c}$ represent the nonlinear Coulomb frictions at the motor side and the load side, respectively. d_{fm} and $d_{f\ell}$ represent the additional repetitive disturbances at the motor side and the load side, respectively. $\tilde{\theta}$ is the transmission error of the harmonic drive, which is defined as the deviation between the expected reducer output position and the actual reducer output position. It can be approximated with a simple sinusoid as $\tilde{\theta} = A\sin(2\dot{\theta}_m t + \phi)$, where A is the amplitude of the transmission error, ϕ is the phase, and the frequency is 2 times the motor side velocity [12].

The dynamic model for this setup can be formulated as

$$J_m \ddot{\theta}_m + d_m \dot{\theta}_m = u + d_1 - \frac{1}{N}\left[k_j \left(\frac{\theta_m}{N} - \theta_\ell \right) + d_j \left(\frac{\dot{\theta}_m}{N} - \dot{\theta}_\ell \right) \right]$$

$$J_\ell \ddot{\theta}_\ell + d_\ell \dot{\theta}_\ell = k_j \left(\frac{\theta_m}{N} - \theta_\ell \right) + d_j \left(\frac{\dot{\theta}_m}{N} - \dot{\theta}_\ell \right) + d_2$$

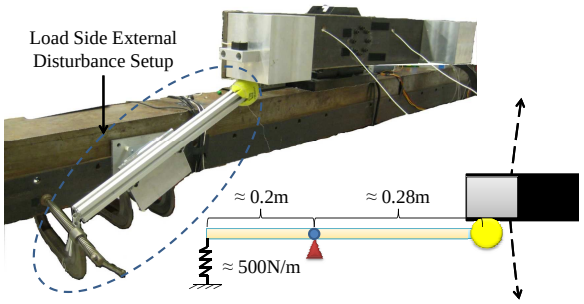

FIGURE 3. Load Side Disturbance Setup for Single-Joint System

where

$$d_1 = d_{fm} - f_{mc}\text{sgn}(\dot{\theta}_m) + \frac{1}{N}\left(k_j\tilde{\theta} + d_j\dot{\tilde{\theta}}\right)$$
$$d_2 = d_{f\ell} - f_{\ell c}\text{sgn}(\dot{\theta}_\ell) - \left(k_j\tilde{\theta} + d_j\dot{\tilde{\theta}}\right)$$

Therefore, the above indirect drive model can be considered as a mismatched system described in (3)-(4) with the disturbance $d = \begin{bmatrix} d_1 & d_2 \end{bmatrix}^{\mathrm{T}}$. The two outputs q_m and q_ℓ are the motor side position θ_m and the load side position θ_ℓ, respectively. Note that d is repetitive if q_m and q_ℓ are repetitive. The continuous time transfer functions from the inputs to the outputs become

$$P_{mu}(s) = \frac{J_\ell s^2 + (d_j + d_\ell)s + k_j}{J_m J_\ell s^4 + J_d s^3 + J_k s^2 + k_j(d_m + d_\ell/N^2)s} \quad (34)$$
$$P_{\ell u}(s) = \frac{d_j s + k_j}{N\left[J_m J_\ell s^4 + J_d s^3 + J_k s^2 + k_j(d_m + d_\ell/N^2)s\right]} \quad (35)$$
$$P_{md_2}(s) = \frac{d_j s + k_j}{N\left[J_m J_\ell s^4 + J_d s^3 + J_k s^2 + k_j(d_m + d_\ell/N^2)s\right]} \quad (36)$$
$$P_{\ell d_2}(s) = \frac{J_{mi} s^2 + (d_j/N^2 + d_m)s + k_j/N^2}{J_m J_\ell s^4 + J_d s^3 + J_k s^2 + k_j(d_m + d_\ell/N^2)s} \quad (37)$$
$$P_{md}(s) = \begin{bmatrix} P_{mu}(s) & P_{md_2}(s) \end{bmatrix}, \quad P_{\ell d}(s) = \begin{bmatrix} P_{\ell u}(s) & P_{\ell d_2}(s) \end{bmatrix} \quad (38)$$

where

$$J_d = J_m(d_j + d_\ell) + J_\ell\left(\frac{d_j}{N^2} + d_m\right) \quad (39)$$
$$J_k = J_m k_j + \frac{J_\ell k_j}{N^2} + (d_j + d_\ell)d_m + \frac{d_j d_\ell}{N^2} \quad (40)$$

System Disturbance Characteristics

In this setup, the identified Coulomb friction combined at the motor side (i.e., $f_{mc} + \frac{f_{\ell c}}{N^2}$) is about 0.1004Nm. A fictitious torque is added in the motor torque command to simulate the external disturbance d_{fm} at the motor side. In the following experiments, d_{fm} is set as a 1Hz sinusoid starting from 3sec with an amplitude of 0.2Nm, i.e., $d_{fm} = 0.2\sin(2\pi(t-3))$Nm. The repetitive external disturbance $d_{f\ell}$ at the load side is generated using the setup shown in Fig. 3. It is designed to have the extension springs apply a maximum disturbance of approximately 20Nm at the load side when the payload hits the ball and continues rotating for about 14 degrees.

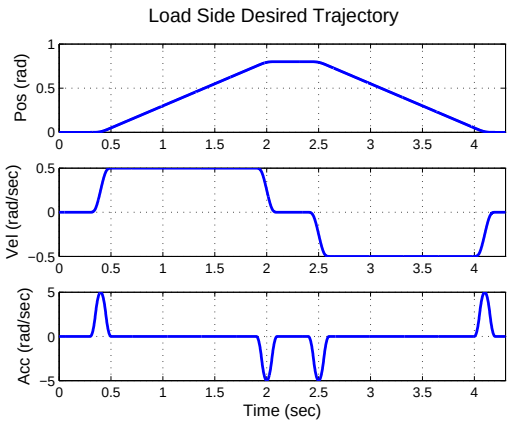

FIGURE 4. Load Side Desired Trajectory

The motor side feedback controller C designed for this setup has a resonant frequency at about 11Hz for the velocity loop. This corresponds to about 1 rad/sec at the load side. Therefore, in order to amplify the transmission error effects, the load side desired trajectory is designed to have a speed of 0.5 rad/sec for most time so that the resulting transmission error frequency will coincide with the resonant frequency of the velocity loop . The resulting trajectory is shown in Fig. 4, which is designed as a fourth-order time optimal trajectory suggested in [13].

The effects of these different kinds of disturbances on the load side tracking performance with the basic controller structure (i.e., C, F_1, and F_2 in Fig. 1) are illustrated in Fig. 5.

Algorithm Setup

The zero-phase acausal low-pass filters Q_r and Q_u are obtained as $Q_r(z) = Q_u(z) = Q_1(z^{-1})Q_1(z)$, where $Q_1(z)$ is a low-pass filter with a cut-off frequency of 30Hz, which is beyond the system elastic anti-resonant and resonant frequencies. With this selection of $Q_r(z)$ and $Q_u(z)$, the frequency responses of β_r in (20) and β_u in (27) with $\pm 50\%$ parametric uncertainties are plotted in Fig. 6 to verify the monotonic stability condition.

Figure 6 shows that, using either motor side model or load side model, the magnitudes of β_r and β_u are always below 0dB indicating $\beta_r < 1$ and $\beta_u < 1$. Therefore, the monotonic stabilities (20) and (27) are ensured separately for both ILC schemes.

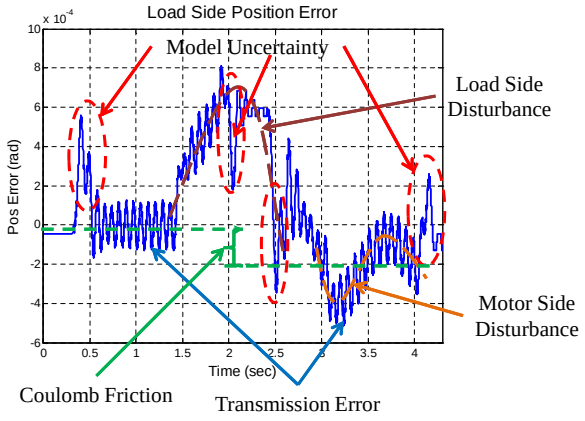

FIGURE 5. Disturbance Effects on Load Side Position Tracking Error

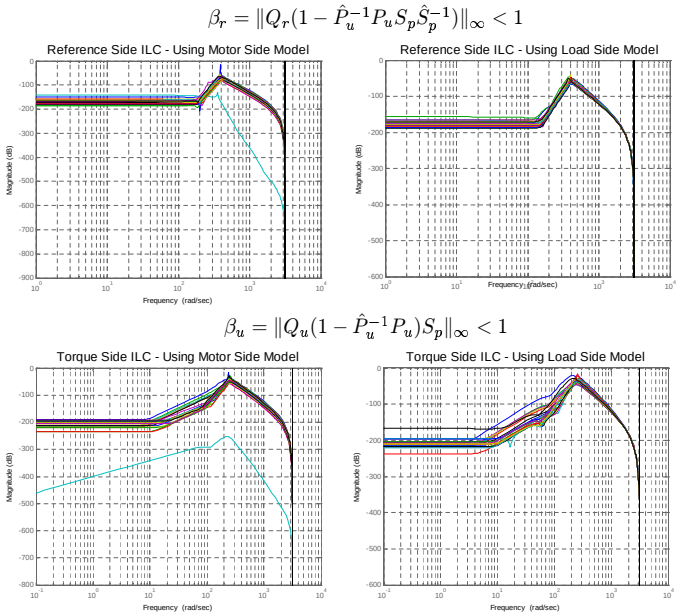

FIGURE 6. Frequency Responses of β_r and β_u with $\pm 50\%$ Parametric Uncertainties

Now consider the two-stage approach proposed in [6]. It can be shown that, the approach in [6] with plant inversion learning filters can be reformulated similarly as the reference ILC (L) with $\hat{P}_u = \hat{P}_{\ell u}$ plus the torque ILC (M) with $\hat{P}_u = \hat{P}_{mu}$ in this paper. This means that the two-stage ILC scheme is performed with mismatched nominal models. As expected, this will not help to attenuate the model uncertainty but instead may even deteriorate the ILC convergence performance. To see this, the tracking performances in the following experiments will be compared in three controller settings, i.e., reference ILC with $\hat{P}_u = \hat{P}_{\ell u}$ only (RefILC(L)), reference ILC with $\hat{P}_u = \hat{P}_{\ell u}$ plus torque ILC with

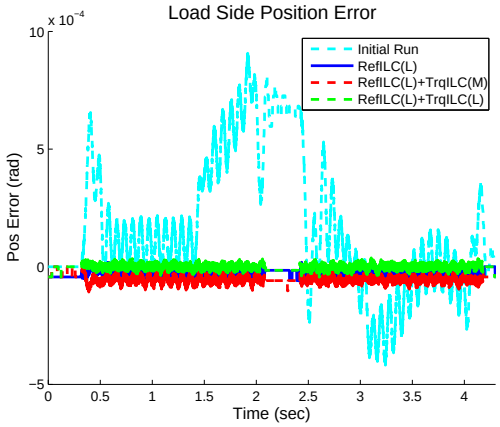

FIGURE 7. Performance Comparisons using Accurate Nominal Model (After 10 Iterations)

$\hat{P}_u = \hat{P}_{mu}$ (RefILC(L) + TrqILC(M)), and reference ILC with $\hat{P}_u = \hat{P}_{\ell u}$ plus torque ILC with $\hat{P}_u = \hat{P}_{\ell u}$ (RefILC(L) + TrqILC(L)).

Experimental Results

Each controller setting is implemented to track the load side desired trajectory in Fig. 4 for 10 iterations. First, the nominal model with accurately identified system dynamic parameters is used in the controller design. With an accurate nominal model, it is expected that the three controller settings will perform equally well. As shown in Fig. 7, the load side position tracking errors for these three settings are all significantly reduced to almost the level of load side encoder resolution.

Next the three controller settings are compared using the nominal model with 15% uncertainty in the dynamic parameters. Normally, with larger model uncertainties, the cut off frequencies of Q filters need to be reduced to ensure the convergence of the learning process. Here, the Q filters are kept the same as the previous case in order to verify the benefits of the proposed scheme. Fig. 8(a) shows that the torque ILC performs very well once it is activated. No matter which nominal model is chosen to follow, the model following errors are greatly reduced with fast convergence rate. As to the load side tracking performance, however, more differences are expected. It is shown in Fig. 8(b) that, due to the model uncertainty, the setting RefILC(L) does not perform as well as before. The setting RefILC(L)+TrqILC(M) actually deteriorates the performance since TrqILC(M) is intended to make the inner plant match with the motor side nominal model while the load side behavior may actually deviate further from its nominal behavior. In contrast, the setting RefILC(L)+TrqILC(L) performs the best since it intends to make the inner plant behave as the load side nominal model and thus greatly releases the uncertainty burden on the reference ILC.

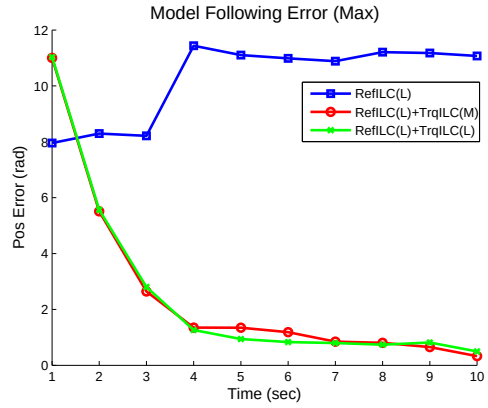

(a) Model Following Error Convergence

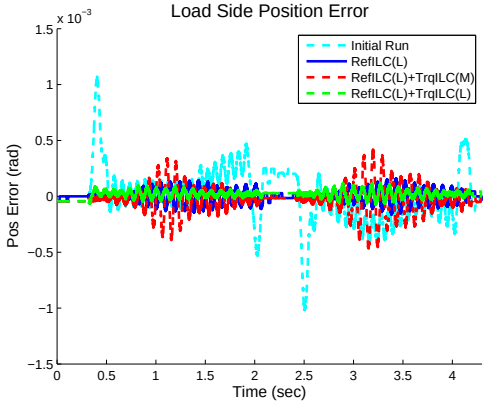

(b) Load Side Position Tracking Error

FIGURE 8. Performance Comparisons using Nominal Model with 15% Parametric Uncertainties (After 10 Iterations)

CONCLUSIONS

In this paper, a model based two-stage ILC scheme was developed for a class of MIMO mismatched linear systems. To improve the performance of the ILC stage aimed for tracking error reduction, another ILC utilizing the idea of model following was designed to drive the inner plant to behave like the nominal model. The convergence property was investigated with proper Q filter and learning filter design. In order to make the two ILC stages work properly together, an ad hoc hybrid scheme was proposed to make transitions between the two ILC stages. A single-joint indirect drive system with several inherent and designed external disturbances was utilized to experimentally validate the proposed ILC scheme. It was shown that the proposed hybrid two-stage ILC scheme using the load side nominal model outperformed the other two benchmark controller settings in the load side tracking application. The application extension of this work to a 6-joint robot manipulator has also been conducted and the results will be reported in [14].

REFERENCES

[1] Bristow, D. A., and Tharayil, M., 2006. "A survey of iterative learning control: A learning-based method for high-performance tracking control". *IEEE Control Systems Magazine*(June), pp. 96–114.

[2] Arimoto, S., Kawamura, S., and Miyazaki, F., 1984. "Bettering operation of Robots by learning". *Journal of Robotic Systems*, ***1***(2), pp. 123–140.

[3] Hassan K. Khalil, 2002. *Nonlinear Systems*. Prentice Hall.

[4] Hedrick, J. K., and Yip, P. P., 2000. "Multiple Sliding Surface Control: Theory and Application". *Journal of Dynamic Systems, Measurement, and Control*, ***122***(4), p. 586.

[5] Yao, B., and Tomizuka, M., 2001. "Adaptive robust control of MIMO nonlinear systems in semi-strict feedback forms". *Automatica*, ***37***(9), pp. 1305–1321.

[6] Miyazaki, F., Kawamura, S., Matsumori, M., and Arimoto, S., 1986. "Learning control scheme for a class of robot systems with elasticity". In Proceedings of the 25th IEEE Conference on Decision and Control,, pp. 74–79.

[7] Wada, M., Tsukahara, T., Tsuda, K., Electric, F., and Division, E. D., 1993. "Learning Control of Elastic Joint Robot and its Application to the Industrial Robot Manipulator". In Proceedings of the IEEE International Conference on Robotics and Automation, pp. 417–422.

[8] De Roover, D., and Bosgra, O., 2000. "Synthesis of robust multivariable iterative learning controllers with application to a wafer stage motion system". *International Journal of Control*, ***73***(10), pp. 968–979.

[9] Owens, D., Hatonen, J., and Daley, S., 2009. "Robust monotone gradientbased discretetime iterative learning control". *International Journal of Robust and Nonlinear Control*, ***19***, pp. 634–661.

[10] Hakvoort, W., Aarts, R., van Dijk, J., and Jonker, J., 2007. "Model-based iterative learning control applied to an industrial robot with elasticity". In Proceedings of IEEE Conference on Decision and Control, pp. 4185–4190.

[11] Padieu, F., and Su, R., 1990. "An H_∞ approach to learning control systems". *International Journal of Adaptive Control and Signal Processing*, ***4***(6), Nov., pp. 465–474.

[12] Han, C.-H., Wang, C.-C., and Tomizuka, M., 2008. "Suppression of vibration due to transmission error of harmonic drives using peak filter with acceleration feedback". In Proceedings of the 10th IEEE International Workshop on Advanced Motion Control, pp. 182–187.

[13] Lambrechts, P., Boerlage, M., and Steinbuch, M., 2005. "Trajectory planning and feedforward design for electromechanical motion systems". *Control Engineering Practice*, ***13***(2), pp. 145–157.

[14] Chen, W., and Tomizuka, M., 2012. "Iterative Learning Control with Sensor Fusion for Robots with Mismatched Dynamics and Mismatched Sensing". In 2012 ASME Dynamic Systems and Control Conference, under review.